PRAMANA
—journal of
physics

Vol. 50, No. 6,
June 1998
pp. 653–668

Metal-ion implantation in glasses: Physical and chemical aspects

F CACCAVALE
Istituto Nazionale per la Fisica della Materia (INFM) and University of Padova, Physics Department, via Marzolo 8, 35131 Padova, Italy
E-mail: caccavale@padova.infm.it

Abstract. A review of the state-of the-art of the research in the field of chemical interactions in silica and silicate glasses implanted with metal ions (e.g., Si, Ti, W, Ag, Cu, Cr) and N is presented in terms of new compounds formation. Moreover, under certain circumstances, the formation of nanometer-radius metal colloidal particles in a thin surface layer is observed. The chemical state of the implanted atoms is determined by X-ray photoelectron (XPS) and X-ray excited Auger-electron spectroscopies (XE-AES). Rutherford backscattering spectrometry (RBS) and secondary-ion mass spectrometry (SIMS) are used to determine the in-depth elemental distributions. Optical absorption measurements and transmission electron microscopy (TEM) are used to detect the presence of metallic clusters, as well as to determine their mean size and size distribution. A thermodynamics approach is used to explain the interaction between the implanted ion and the separate atomic species of the target glass and/or between the implanted ion and the target molecular species.

Keywords. Ion implantation; glass; chemical interaction; compound formation; metal nanoclusters.

PACS No. 34.50; 61.43; 61.46; 61.72

1. Introduction

Because of its unique features, research on ion implantation in insulators grew independently from works in the field of metals and semiconductors since the first years of 1970. Ion implantation in glasses attracted a large interest being one of the most attractive methods to incorporate virtually any element in a substrate and for the possibility to overcome the doping solubility limits.

The interaction of energetic ions with an insulating glass target determines effects directly connected to radiation damage, such as mechanical stresses, density and composition modifications, and consequent mechanical, optical and chemical durability property changes [1, 2]. In addition to these, depending on the choice of element and dielectric host, chemical interactions with the formation of particular compounds are possible [3–5].

The chemical role in determining the final properties of the implanted layers was first observed in experiments employing the double implantation of nitrogen and silicon in silica glasses [6–9]. Implantation of metal ions into glass is of particular interest since, depending on their reactivity with the substrate, they cause the synthesis of new compounds [10–13], and/or the formation of metallic nanoclusters [5, 11, 12, 14, 15].

The group of Padova is active in the study of the chemical interactions in SiO_2 and silicate glasses implanted with metal ions with the aim of giving a contribution to the

understanding of the processes governing the interaction between the dielectric host and the implanted element. In the present review results obtained for SiO_2 and silicate glasses implanted with metals of different reactivity, i.e. silicon, titanium, tungsten, silver, copper and chromium are presented. Some of these samples have been successively implanted with nitrogen ions.

Results are explained by using a two-step model where the ballistic effects are separated from the chemical (thermodynamic) driving forces. The thermodynamic approach to explaining the chemical interactions between implanted species and the substrate presents some uncertainty, due to the correct values of the 'local' temperature and, consequently of the Gibbs energy (ΔG^0). Moreover it is necessary to ascertain if the interaction is between the implanted ion and the separate atomic species of the target glass or between the implanted ion and the target molecular species. The ΔG^0 values may be very different in the two cases [16].

The chemical state of the implanted metals is determined by X-ray photoelectron (XPS) and X-ray excited Auger-electron spectroscopies (XE-AES). Rutherford backscattering spectrometry (RBS) and secondary-ion mass spectrometry (SIMS) is used to determine the in-depth elemental distributions, getting smooth and accurate concentration profiles up to several micrometers. Optical absorption measurements and transmission electron microscopy (TEM) are used to detect the presence of metallic clusters, as well as their mean size and size distribution. Experimental details are reported in previous papers [3, 10, 11].

2. Results and discussion

2.1 *Nitrogen and silicon+nitrogen implanted SiO_2*

Three typical SIMS profiles of nitrogen in 50 keV N-implanted SiO_2 samples are shown in figure 1 [3]. Specimens implanted at low doses (between 2.5×10^{15} and $1 \times 10^{16}\,cm^{-2}$) show nitrogen distributions peaked at a depth in agreement with the expected R_p value. At doses close to $5 \times 10^{16}\,cm^{-2}$ the top of the N profile begins to be flat. Further increasing the dose, the nitrogen profile exhibits a long plateau, which extends from the surface up to depths much greater than the $R_p + \Delta R_p$, and increases with increasing dose [17]. Above $5 \times 10^{16}\,cm^{-2}$ the total nitrogen amount retained in the sample begins to be significantly lower than the nominal implantation dose and eventually saturates at a value close to $1 \times 10^{17}\,cm^{-2}$. Nitrogen in excess of this value is desorbed during implantation.

The XPS analysis of the Si2*p* and N1*s* lines in implanted samples show binding energy (BE) peaks which can be associated with the formation of both silicon oxynitrides and nitrogen gaseous compounds [6].

The implant of silicon in SiO_2, besides the radiation damage of the substrate, introduces an excess of Si atoms with the consequent formation of substoichiometric SiO_x oxides and metallic silicon clusters. These species are chemically reactive, hence a pronounced interaction between them and the successively implanted nitrogen are expected. Figure 2 [3] compares the SIMS profiles of samples implanted at first with ^{29}Si and successively with nitrogen at 50 keV or 100 keV. In the silicon+nitrogen (100 keV) implanted sample the distribution of nitrogen follows that of ^{29}Si and shows a peak at a concentration much higher than the saturation level of the flat profiles observed in

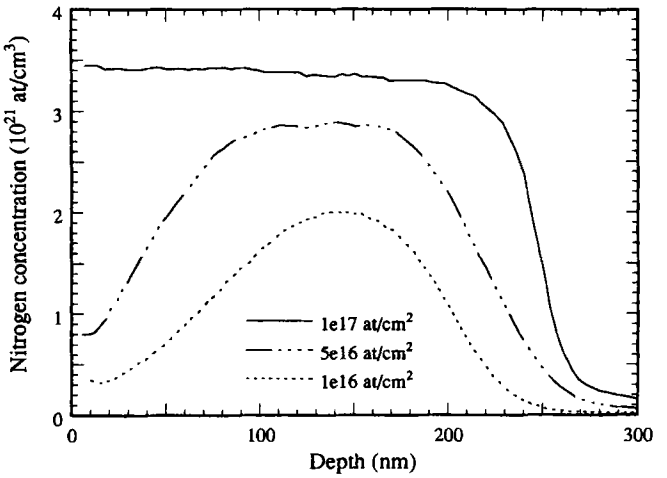

Figure 1. SIMS depth profiles of nitrogen implanted in silica at 50 keV and different doses.

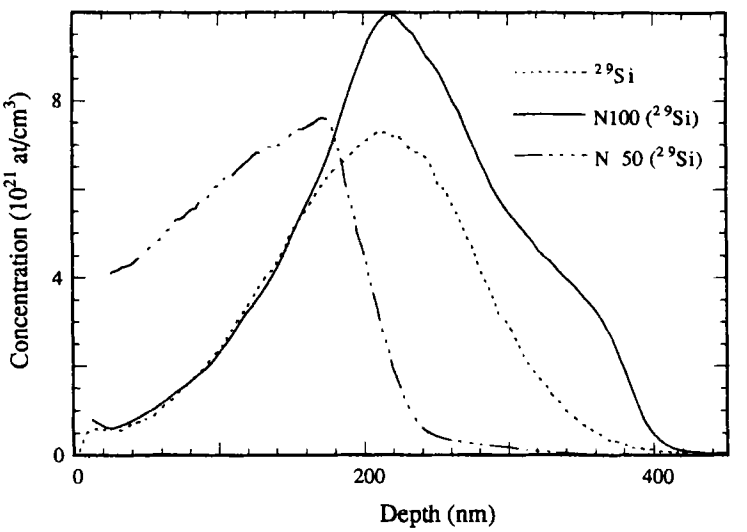

Figure 2. SIMS depth profiles of ^{29}Si and nitrogen implanted in SiO_2 at 50 and 100 keV in ^{29}Si+N-implanted sample.

only-nitrogen implanted specimens. The nominal nitrogen dose is almost totally (i.e. about 90%) retained and only a minor deformation in the shape of the N profile towards higher depths is visible and is connected to the large penetration depth of the nitrogen ions with this energy. At a lower implantation energy (50 keV) for nitrogen, its concentration increases, following the implanted silicon distribution, from a low value, close to the surface, to a large one at a depth of about 200 nm and then drops of more than one order of magnitude between 200 and 250 nm. Because of the more shallow

implantation depth and of the lower excess of implanted Si atoms here present, some out-diffusion of N takes place in this latter case with respect to the higher energy nitrogen implantation.

A N/N+O atomic ratio value of 0.25 has been determined close to the maximum of the implanted silicon distribution by XPS. Moreover, while the N1*s* peak of the oxynitride increases in intensity with depth, the peak attributed to molecular nitrogen does not. This suggested that the formation of molecular nitrogen precipitates is related to the radiation damage, but also that radiation damage plays a secondary role when chemical interactions can occur [3].

2.2 *Titanium and titanium+nitrogen implanted SiO_2*

The implantation of titanium in SiO_2 introduces a very reactive element in a chemically stable matrix and radiation damage of the substrate. In general, titanium silicides are well known stable compounds. According to thermodynamic considerations, the following reaction is allowed [18]

$$x\mathrm{Ti} + \mathrm{SiO_2} \rightarrow \mathrm{Ti}_y\mathrm{Si} + \mathrm{Ti}_{x-y}\mathrm{O_2};$$

thus, one can expect strong interactions between the implanted Ti atoms and the host matrix.

After implantation of 30 keV Ti in SiO_2, the XPS spectrum of the unresolved Si2*p* doublet (figure 3 [10]), at different depths from the surface up to a depth of about $2R_p$, shows two distinct components. One corresponds to the silica matrix, the other is consistent with the presence of titanium silicide.

The XPS analysis of Ti2*p* and O1*s* BE peaks confirmed the formation of both titanium oxide (TiO_2) and titanium silicide ($TiSi_x$, with variable stoichiometry) species [10]. In particular, above a concentration of about 20 at.%, the amount of titanium atoms in the silicide species exceeds the amount of Ti atoms in the oxide one. An oxygen depletion to a depth close to the maximum titanium concentration was also detected.

Thermodynamic evaluation of ΔG^0 for the reactions

$$2\mathrm{Ti} + \mathrm{SiO_2} \rightarrow \mathrm{TiSi} + \mathrm{TiO_2},$$
$$8\mathrm{Ti} + 3\mathrm{SiO_2} \rightarrow \mathrm{Ti_5Si_3} + 3\mathrm{TiO_2}$$

suggests only that the formation of both TiSi and Ti_5Si_3 species is possible.

The formation of TiSi or Ti_5Si_3 is expected to depend on titanium local concentration. In particular, near R_p, the Ti_5Si_3 compound should be favoured with respect to TiSi. However, oxygen loss due to radiation damage can play a role in determining the final product ratio (tisilicide/tioxide). There is no evidence of metallic titanium and/or silicon formation. At the same time at depths larger than $R_p + \Delta R_p$, an oxygen excess was observed even if TiSi is still present. This oxygen excess is probably connected to the displaced oxygen atoms which migrate toward the bulk following the radiation damage.

On the basis of the above results, and in agreement with a model proposed by Kelly [19], the mechanism involved in Ti implantation in silica can be correctly described on the basis of the following two-step model:

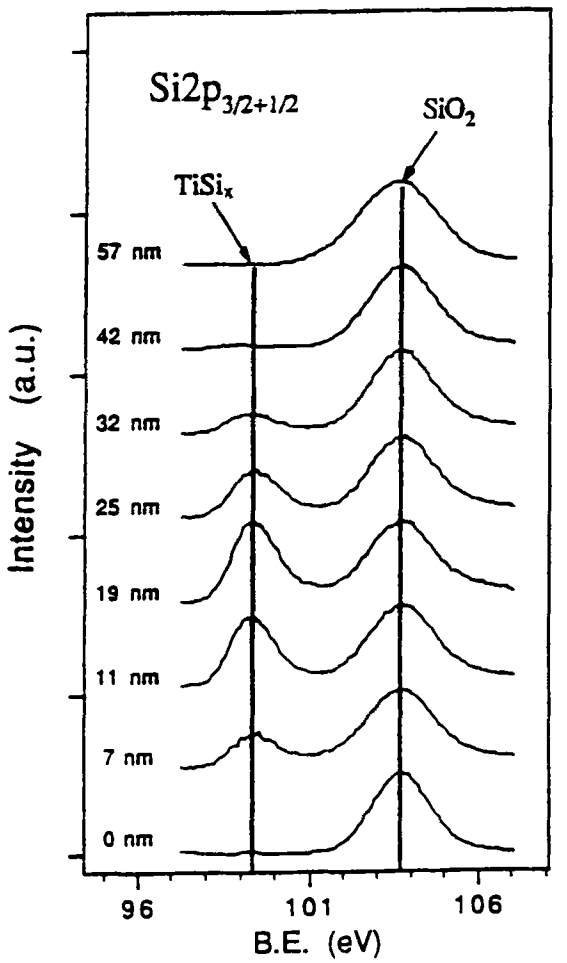

Figure 3. XPS spectrum of the Si($2p_{3/2+1/2}$) doublet, at different depth from the surface up to a depth of 57 nm in 30 keV Ti-implanted SiO_2.

(1) a high energy ballistic process where titanium atom implantation will cause an oxygen depletion generating substoichiometric silica (SiO_x) at depths lower than R_p;
(2) a low energy, chemically (i.e., thermodynamically) guided, process which gives rise to $TiSi_x$ and TiO_2 products.

Thermodynamic considerations favour the formation of titanium silicides with respect to pure metallic Ti and Si.

The TEM analysis of the 30 keV Ti implanted samples revealed the presence of small TiSi clusters very close to the surface. The largest clusters have diameters of about 20 nm and they appeared to be amorphous from the electron microdiffraction. The obtained relative concentration was [Ti]/[Si]= 1.1 ± 0.3 [12].

Figure 4 shows the SIMS profiles of samples implanted first with 190 keV titanium and successively with 40, 70 and 100 keV nitrogen. Only minor modifications in the titanium

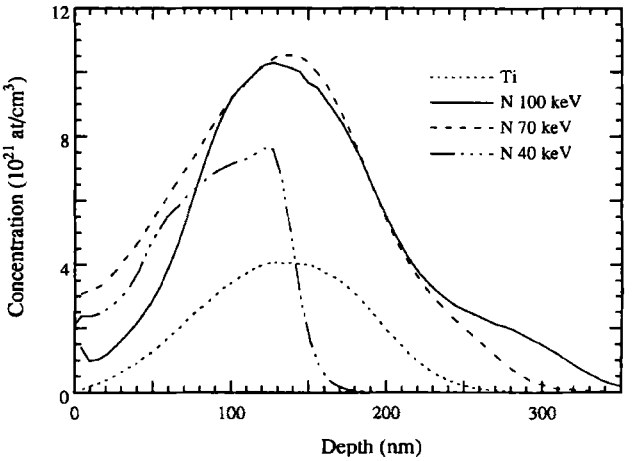

Figure 4. SIMS depth profiles of Ti and N implanted in SiO_2 at 40, 70 and 100 keV in Ti+N-implanted sample.

concentration profiles are detectable as a function of the nitrogen implantation conditions; on the other hand nitrogen profiles are strictly related to those of titanium, in a way similar to that observed for the silicon+nitrogen implanted samples. When N is implanted at 40 keV its concentration increases as that of Ti increases and drops quite sharply when the effective maximum penetration depth for the nitrogen ions is reached. A large part of the implanted nitrogen (about 50%) was desorbed. For the 70 keV N implantation the shape of the nitrogen concentration profiles matches that of Ti. For deeper nitrogen implants (100 keV) the N concentration profile follows that of Ti, with a tail at larger depth which indicate the maximum penetration depth of nitrogen at this energy.

The more striking effect of the N implant in low energy Ti pre-implanted samples is the disappearance of the TiSi species. In fact the Ti2*p* and Si2*p* XPS peaks corresponding to TiSi are no more present after the N implant. Moreover, the depth profile of N follows the Ti profile making evident the interaction between these two elements. The N interaction with the Ti-implanted silica can be summarized as follows

$$N + TiO_2 \rightarrow TiO_xN_y + N_2,$$
$$N + TiSi_x \rightarrow Ti_{met} + SiN_z.$$

From a thermodynamic point of view, no significant differences in ΔG^0 can be calculated for the nitrogen interaction with titanium silicide to obtain titanium and silicon nitrides or metallic titanium and silicon nitride.

2.3 *Tungsten and tungsten+nitrogen implanted SiO_2*

While tungsten is less reactive than titanium, its peculiarity is to form clusters and structurally disordered oxides with chemically inequivalent metallic centres. The tendency of W in its higher oxidation states to polymerize and form bridges and/or direct bonds with other metals is well known. Thermodynamic considerations applied to this system

suggest that silicide species formation is not favoured in this case. In particular the reaction

$$3W + 2SiO_2 \rightarrow WSi_2 + 2WO_2;$$

is thermodynamically allowed but less favoured than formation of tungsten metallic precipitates:

$$3W + SiO_2 \rightarrow W_{met} + SiO_2.$$

As a consequence, the implantation of tungsten in silica will involve primarily precipitation of metallic W and no silicide formation.

From the XPS analysis of the W4*f*, Si2*p* and O1*s* line peaks at implantation dose of 5×10^{16} cm^{-2} metallic W precipitates as well as tungsten oxides (WO_2 and mixed WO_x–SiO_2) have been detected [10].

At variance with the experimental evidence present in the Ti-implanted silica, the W implantation does not induce oxygen depletion up to R_p, as observed from XPS and RBS analyses. At depths larger than R_p, however, the Ti and W implantation induce the same effect, i.e., an oxygen increase to be related to displaced oxygen atoms which migrate toward the bulk following the radiation damage. This could imply formation of tungsten oxides, which from a thermodynamic point of view are disfavoured, due to radiation damage during the ballistic step and oxygen migration from the atmosphere. This interpretation explains the large amount of tungsten oxides and the corresponding absence of a silicon signal at the proper binding energy for any silicide or metallic silicon species.

Nitrogen implantation of the W-implanted sample seemed to induce some variation in the W4*f* XPS peak only in terms of relative intensity. From the analysis of both N1*s* and Si2*p* lines it results that after N implantation only tungsten oxynitride is present. However, the thermodynamic evaluation of the expected products of nitrogen introduced in the W-implanted silica network is unattainable because no data are available for silicon and tungsten oxynitride species.

2.4 *Silver and silver+nitrogen implanted SiO_2*

Silver does not react with SiO_2, hence we do not expect strong interactions of the implanted silver atoms with both the host matrix and the successively implanted nitrogen atoms.

The RBS profile of Ag implanted in silica has a nearly-Gaussian shape, but slightly broader than the calculated one and with an appreciable amount of atoms present at the surface (see figure 5, [3]). This effect is due to the very high mobility of Ag in SiO_2, mobility which is enhanced by the radiation damage. The successive implant of 50 keV N ions causes an impressive modification of the silver profile: near the surface and at a depth comparable to the nitrogen projected range silver is completely depleted, it accumulates, forming sharp peaks, very close to the previous position of the maximum concentration and at a depth larger than $R_p + \Delta R_p$ value of the nitrogen ions. About one half of the implanted Ag disappears. The implant of 100 keV N ions, being deeper than the region where silver atoms are located, does not cause a depletion within the Ag profile, but a narrowing of the silver distribution around the depth at which the maximum concentration occurred. About one third of the implanted Ag atoms is lost now.

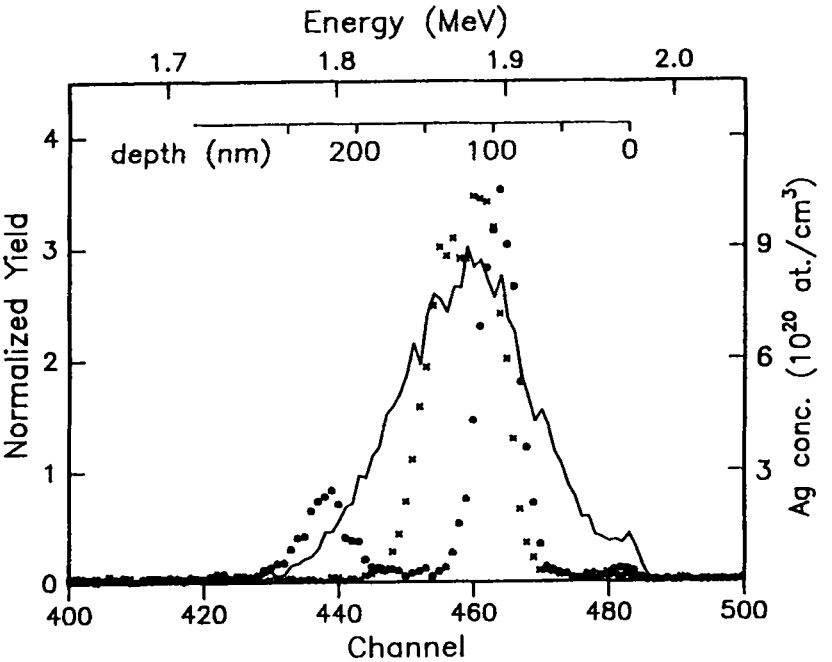

Figure 5. RBS signals of silver, in Ag-implanted SiO_2 (—) before and after the implantation of nitrogen at the energies of (•) 50 and (x) 100 keV.

What has been observed is consistent with the competition of two mechanisms: (i) a diffusion of Ag atoms, coupled with radiation-induced defects, which results in the depletion of silver in the region where nitrogen ions deposit the most part of their energy and a migration to the surface where Ag is preferentially sputtered; and (ii) the aggregation of the dispersed silver atoms to form metallic colloidal particles which are no more mobile under the defect flux. The latter phenomenon is responsible for the narrowing of the silver distribution around the position where the maximum in the concentration occurs. SIMS analysis of the nitrogen concentration profiles shows that in all cases the N depth distribution is not influenced by the silver profile and is flat up to the maximum nitrogen penetration depth, as observed in the samples implanted only with nitrogen (see above).

The hypothesis of noninteraction between the implanted silver atoms and the host matrix is confirmed by the XPS analysis. The silver distribution does not modify the silicon and oxygen concentration profile. From the analysis of the Ag3*d* peak position it results that the implanted silver atoms precipitate to form small metallic islands whose dimensions and concentration influences the line position. The successive nitrogen implant does not produce a chemical, but mainly a physical effect by contracting the Ag distribution.

Colloidal silver precipitates should give an optical absorption band centred at a wavelength of about 400 nm. This is what occurs in our samples. The optical absorption of samples implanted with Ag and Ag+N ions is shown in figure 6 [3]. An appreciable absorption already occurs in the sample implanted only with silver, as observed also by Arnold [20]. This can be attributed to part of the implanted atoms which precipitate during

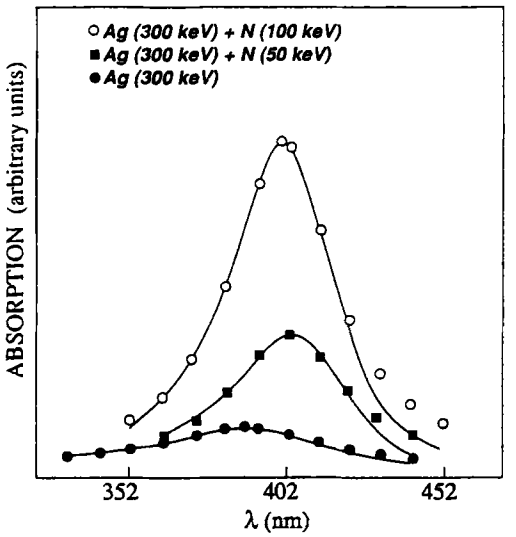

Figure 6. Optical absorption peak, as a function of wavelength, for Ag and Ag+N implanted SiO_2.

the implantation near the maximum concentration, favoured in doing this by the radiation enhanced diffusion.

The successive N implantation, beside causing the loss of silver observed in the RBS spectra, favours the increase in number and size of these colloidal particles (as a consequence the intensity of the absorption band increases) by enhancing the Ag diffusion by radiation and beam heating effects.

2.5 *Copper implantation*

2.5.1 *Fused silica samples*: In copper-implanted SiO_2, the copper depth concentration profile, reported in figure 7, shows the usual bimodal character [11]. It results from the analysis of the XPS Cu2*p* and XE-AES CuLMM signals that in the region where atomic copper percentage exceeds 2% the presence of metallic Cu as well as dispersed oxidized copper atoms. The optical absorption spectrum of this sample confirms the presence of metallic precipitates: it displays an absorption band peaked at a wavelength of about 560 nm, typical for surface plasmon resonance in copper quantum dots. It results from TEM analysis that copper clusters have a mean diameter of 6.5 ± 1.5 nm with a fcc structure, corresponding to lattice parameters of elemental copper crystals and are randomly oriented.

2.5.2 *Soda-lime glass samples*: In the soda-lime glass the copper depth concentration profile, reported in figure 8 [11] is approximately Gaussian in shape. At the same time the sodium profile displays a typical depletion connected to the radiation-enhanced diffusion of the alkaline element and its preferential sputtering during implantation [21].

XPS and XE-AES copper signals for this sample are the same seen for fused silica with the same concentration dependence. No relationship between the chemical state of Cu

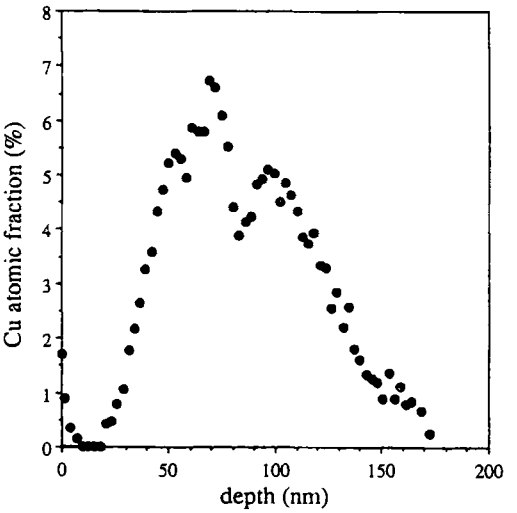

Figure 7. Copper depth profile, obtained by XPS, in Cu-implanted SiO_2.

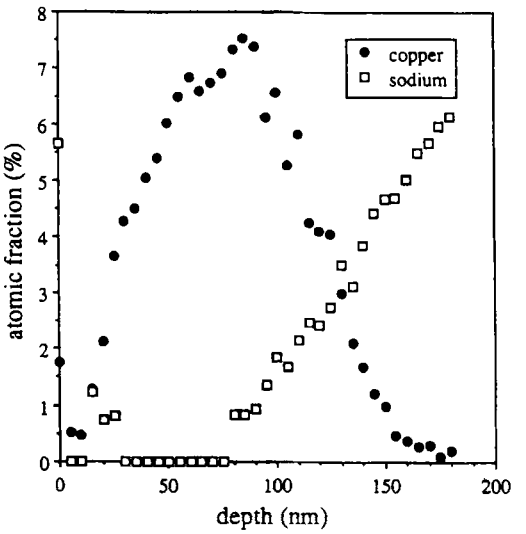

Figure 8. Cu and Na depth profiles, obtained by XPS, in Cu-implanted soda-lime glass.

atoms and Na concentration is evident: the atomic sites left free by sodium atoms seem not to influence the metal colloid formation, since this formation takes place only where the copper concentration exceeds the 2% threshold. TEM measurements confirmed the presence of metallic precipitates whose diameter distribution is peaked about 4.5 ± 1.5 nm, with a structure similar to that already observed in copper-implanted fused silica. Nevertheless, optical absorption measurements do not show the characteristic absorption band due to surface plasmon resonance. The last is not in disagreement with XPS, XE-AES

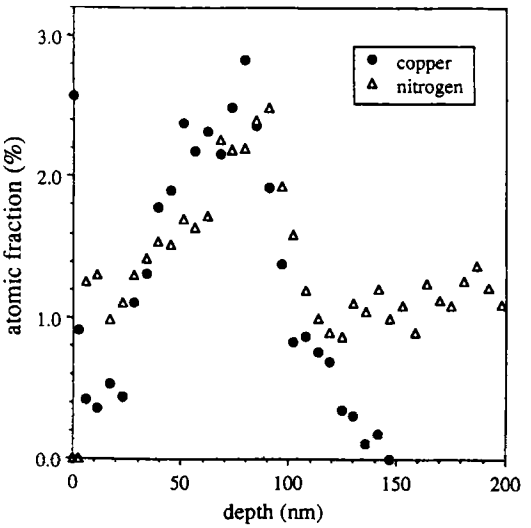

Figure 9. Copper and nitrogen profiles, obtained by XPS, in Cu-implanted soda-lime glass.

and TEM results because of the decrease in the value of the index of refraction of ion-implanted soda-lime glasses mainly related to the near-surface sodium depletion [22]. As a consequence the metallic cluster volume is smaller in soda-lime glass with respect to that in SiO_2 and the copper nanocluster-related absorption is below the sensitivity of the used instrument [11].

2.5.3 *Double implantation in SiO_2 (Cu+N, Cu+Ar)*: The 100 keV nitrogen irradiation in copper-implanted fused silica causes the diffusion of copper towards the surface where it partially accumulates and is sputtered by the incoming ions. Now at every depth the Cu concentration is lower than 3% and the concentration profile, reported in figure 9, shows no bimodal shape. XPS and XE-AES analyses of Cu2*p*, CuLMM and N1*s* signals indicate the formation of nitrides and oxynitrides related to copper. Moreover, the nitrogen depth profile follows the copper distribution and shows a plateau only at depths where Cu is not present. Thus it can be assumed that nitrogen reacts not only with the silica substrate but also with implanted copper causing the dissolution of metal clusters. The absence of a N1*s* XPS component, connected to the formation of molecular nitrogen, is another indication of a large chemical reactivity of N with pre-implanted species.

Optical absorption measurements show no characteristic band indicative of the presence of metallic Cu clusters.

In order to distinguish between chemical and radiation damage effects, a copper-implanted SiO_2 sample was irradiated with argon. Ar implantation parameters were chosen to have energy deposition conditions similar to those of nitrogen implantation. As detected by XPS and XE-AES this argon irradiation does not modify the copper oxidation states compared to the Cu-implanted silica sample. The optical absorption spectrum of the sample confirms the presence of metallic precipitates since the optical absorption band of copper-implanted fused silica sample remains unchanged after Ar implantation. The

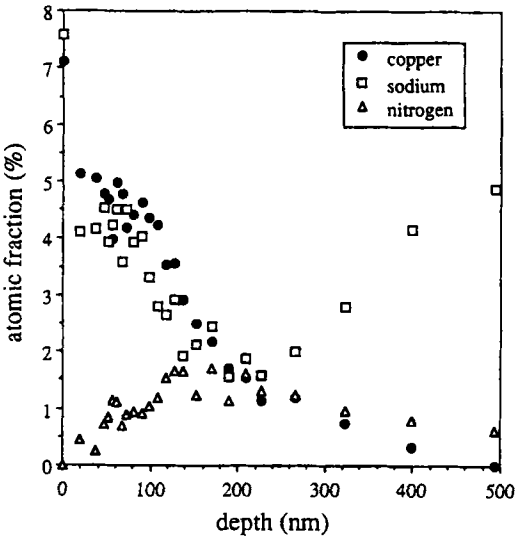

Figure 10. Cu, Na and N depth profiles, obtained by XPS, in Cu+N (100 keV) implanted soda-lime glass.

physical modifications induced by ion implantation alone are unable to induce dissolution of metallic clusters.

2.5.4 *Double implantation in soda-lime glass (Cu+N, Cu+Ar)*: Copper, sodium, and nitrogen depth concentration profiles in the 100 keV nitrogen-irradiated copper-implanted soda-lime glass are reported in figure 10 [11]. A movement of copper atoms towards the surface is again evident, with a loss of Cu because of sputtering. The maximum copper concentration is now about 5 at.%.

Since the nitrogen range in this case well exceeds the depth at which Cu was implanted and sodium formerly depleted, this N irradiation induces also a further movement of sodium resulting in the increase of the width of the sodium depleted layer and an accumulation of Na in the near surface region where copper is also present. There seems to be no correlation between nitrogen and copper profiles, indicating that chemical interactions between Cu and N in this sample are, if present, much weaker than in the case of fused silica subjected to the same implantation conditions.

Sodium and nitrogen profiles are coincident to those measured in a soda-lime glass in the absence of the copper implantation.

From XPS and XE-AES copper spectra the presence of metallic Cu as well as Cu in an 'intermediate' chemical state has been observed. At the surface, all copper atoms are present in the 'intermediate' chemical state. In depth, metallic Cu is present only where the copper concentration is above about 2 at.%. The presence of metallic Cu clusters is confirmed by the presence of the band centred at 560 nm in the optical absorption spectrum. The absence of chemical interaction between Cu and N is confirmed by the B.E. of the N1*s* XPS peak, which is the same in 100 keV N-irradiated soda-lime samples both with and without the Cu implantation. The equality of this value and the near

coincidence of the nitrogen depth profiles in these two cases support the assumption that N reacts only with the host matrix to form silicon oxynitrides (SiO_xN_y, see above).

The appearance of the characteristic optical absorption band in this sample can be tentatively explained by considering that, as a consequence of chemical interactions between nitrogen and the glass matrix, high-refractive index compounds SiO_xN_y are formed in the region where copper is present, thus increasing the extinction coefficient.

Further evidence of the effect of chemical interaction between the substrate and the implanted ions comes from the analysis of the argon irradiation of the copper-implanted soda-lime glass. The copper concentration profile is very similar to that after nitrogen irradiation, while the surface concentration of sodium is now reduced to about 2 at.%. Even if the maximum Cu concentration (4 at.%) is well above the 'solubility threshold', above which in the single copper-implanted samples the metallic Cu precipitation occurs, XPS and XE-AES measurements show that all the copper is present in the form of Cu_2O. Therefore, argon irradiation (only energy deposition without chemical interaction) causes the dissolution of copper clusters. Moreover, in the surface region where Cu moves, sodium-free sites are in excess, thus favoring a bond formation between the copper atoms and oxygen.

The optical absorption measurements show no characteristic absorption band due to metallic copper clusters.

2.6 *Chromium implantation*

The implant of chromium in SiO_2 introduces a reactive element in a chemically stable matrix. Obviously, the radiation damage along the ion track induces large modifications in the target reactivity, improving the chemical interaction between Cr and the target. Chromium oxides are very stable compounds; chromium silicide species are stable compounds as well [23]. Therefore, as a result of silica irradiation with chromium ions, the formation of both chromium oxides and silicides can be expected.

As mentioned above, the chemical interactions in titanium- and tungsten-implanted fused silica lead to the formation of a considerable amount of titanium silicide, even at depths where the relative titanium atomic concentration was only a few percent. At the same time, no tungsten silicide has been detected. From a thermodynamic point of view this is understandable if one observes the Gibbs energy values of these compounds [16]. If we consider the chemical behaviour of Cr with respect to that of Ti and W, we observe that titanium silicide formation is favored with respect to chromium silicide; this latter is more stable than tungsten silicide. As far the oxides, TiO_2 and Cr_2O_3 have similar Gibbs energy values. Therefore, formation of chromium silicide in chromium-implanted silica is expected only when a relatively high value of Cr atomic concentration is present.

XPS analyses show lines that are characteristic of both chromium oxides, in particular of the Cr_2O_3 compound, and chromium silicide species.

3. Conclusions

The formation of titanium silicide and titanium oxide compounds is observed in Ti-implanted silica, in contrast to W implantation which causes the precipitation of metallic

tungsten and the formation of two different types of tungsten oxides. A subsequent nitrogen implantation destroys the $TiSi_x$ species, inducing the formation of Ti metallic clusters and substoichiometric silicon nitrides while interaction between nitrogen and TiO_2 causes the formation of titanium oxynitrides. The N implantation in W pre-implanted silica enables the formation of tungsten oxynitrides. The formation of $CrSi_x$ and Cr_2O_3 species in Cr-implanted silica has also been observed.

These different results are explained by using a two-step model where the physical (ballistic) effects have been separated from the chemical (thermodynamic) driving forces. In particular, the high reactivity of Ti with a local oxygen depletion caused by the implantation damage leads to the formation of elevated quantities of titanium silicide. Thermodynamic considerations indicate that the silicide formation is clearly favoured with respect to metallic titanium and silicon species and its stoichiometry, TiSi or Ti_5Si_3 depends on the local titanium concentration. The subsequent implantation of N destroys titanium silicide, inducing the formation of titanium metallic clusters and substoichiometric silicon nitrides. Interaction between nitrogen and TiO_2 causes the formation of titanium oxynitrides. The experimental findings of metallic precipitates in W-implanted samples also follow the thermodynamic indications, while the formation of oxides can be explained considering both radiation damage during the ballistic step and oxygen migration into the sample from atmosphere toward the initially depleted zone when the tungsten-implanted sample is brought into air. The subsequent implantation of nitrogen causes only partial transformation of metallic precipitates to tungsten oxynitrides.

In the case of silica glass implanted with chromium ions the high-energy ballistic process causes the displacement of oxygen atoms at depths less than the projected range (R_p) via radiation damage; as a consequence oxygen atoms migrate towards the bulk giving rise to an oxygen increase at depths greater than R_p. At the same time the interaction of energetic Cr ions with the substrate can be described by a low-energy process chemically (i.e. thermodynamically) guided, in which chromium oxides and silicides are formed. A satisfactory understanding of the target modifications induced by the chromium ion implantation should also consider the phenomenon of oxygen diffusion from the outermost layers in the low-energy implanted samples.

The thermodynamic approach to explaining the chemical interactions between implanted species and the substrate presents some uncertainty, due to the correct values of the 'local' temperature and, consequently, of the Gibbs energy (ΔG^0). Moreover it is necessary to ascertain if the interaction is between the implanted ion and the separate atomic species of the target glass or between the implanted ion and the target molecular species. The ΔG^0 values may be very different in the two cases. It has been proposed to consider the free energy of oxide formation as the quantity which gives the measure of the chemical interaction, i.e. colloid formation occurs when the Gibbs free energy of formation of oxides of an implanted element M, $\Delta G^0(M_xO_2)$, is greater than that of SiO_2, $\Delta G^0(SiO_2)$. Since ΔG^0 is a function of temperature, a temperature is needed to be specified to compare $\Delta G^0(M_xO_2)$ with $\Delta G^0(SiO_2)$. It has been estimated a fictive temperature in the implanted layer of about 3000 K. This criterion was successfully applied to eleven elements implanted in silica, but important exceptions hinder its general application. In the Ti-SiO_2 system, chemical effects play the major role taking into account that ΔG^0 values for SiO_2 and TiO_2 are comparable. On the other hand, in

the W-SiO_2 system, ΔG^0 values for WO_2 and WO_3 with respect to SiO_2 being much different, the ballistic effects dominate.

Ion implantation of metal ions (e.g. Ag, Cu) in glass substrates leads, under certain circumstances, to the formation of nanometer-radius colloidal particles in a thin surface layer. These particles exhibit an electron plasmon resonance which depends on the optical constants of the implanted metal and on the refractive index of the glass host. Glasses with metal clusters show an enhanced third-order susceptibility $\chi^{(3)}$, whose real part is related to the intensity-dependent refractive index n_2 by $n = 12 * \pi * \mathrm{Re}\chi^{(3)}/n_0$, where $n = n_0 + n_2 I$, n_0 is the linear refractive index and I is the light intensity. Dielectric and quantum confinement effects come into play in defining the nonlinear response of the composites in the picosecond range (fast nonlinearity): the intraband and interband electronic transitions that contribute to the effective $\chi^{(3)}$ turn out to depend strongly on the type of metal, and on the form and size of the clusters, as well as on the metal-dielectric bonds. As a consequence the ion implantation technique may play an important role for the production of all-optical switching devices.

In fused silica, as well as in soda-lime glass, copper implantation gives rise to metallic clusters formation for copper concentration above a threshold value of about 2 at.%. These clusters have different radii largely determined by the irradiated substrate structure. After N implantation the inherent low chemical reactivity of nitrogen with fused silica favors a true chemical interaction between copper and nitrogen, i.e. the formation of copper nitride or oxynitride species dispersed in the matrix. As a consequence, metal precipitates dissolve. On the other hand the higher reactivity of soda-lime glass, due to nonbridging oxygen atoms, favors the interaction between the substrate and nitrogen (SiO_xN_y formation) without dissolution of copper nanoclusters. Argon irradiation of copper-implanted glasses supports the hypothesis of chemically driven interactions. For fused silica the copper clusters remain after argon implantation indicating that the physical effects of irradiation are not sufficient to make the silica substrate reactive with respect to the implanted copper. On the other hand, in the soda-lime glass the depletion of sodium as well as the energy deposition favor interactions between implanted copper and oxygen with the formation of Cu_2O dispersed in the soda-lime matrix.

The presence of amorphous silicide nanoprecipitates as a result of chromium or titanium ion irradiation of silica is detected. It is found that in the Ti-implanted sample a larger amount of silicide species are present in comparison with the Cr-implanted one. Moreover, chemical reactions between the dopant and silicon atoms begin to be detectable at lower dopant concentration in titanium – than chromium – implanted samples. This indicates that Ti-implanted atoms are more reactive than chromium implanted ones in terms of the formation of chemical bonds with silicon of the host silica matrix.

The results achieved up to now and reported in this review are leading us toward a comprehensive understanding of the solid state chemistry of the implanted species in glasses. In the near future we will extend our study to other implanted elements and glass substrates, in order to verify the reliability of the two-step model. The thermodynamic approach supplies satisfactory predictions about chemical modifications of the target. Nevertheless, we are well aware that the ion implantation process does not occur under thermodynamic equilibrium conditions.

Acknowledgements

The author is grateful to G W Arnold, G Battaglin, R Bertoncello, E Cattaruzza, F Gonella, G Mattei, P Mazzoldi and F Trivillin whose results have been extensively used.

References

[1] G W Arnold and P Mazzoldi (eds), in *Ion Beam Modifications of Insulators* (Elsevier, Amsterdam, 1987) p. 222 and references therein
[2] R A Weeks, in *Glasses and Amorphous Materials* edited by J Zarzycki (VCH, Weinheim, 1991) p. 331 and references therein
[3] P Mazzoldi, F Caccavale, E Cattaruzza, A Boscolo-Boscoletto, R Bertoncello, A Glisenti, G Battaglin and C Gerardi, *Nucl. Instrum. Methods* **B65**, 367 (1992)
[4] G Battaglin, in *Modifications Induced by Irradiation of Glasses* edited by P Mazzoldi (Elsevier, Amsterdam, 1992) p. 11 and references therein
[5] P Mazzoldi, G W Arnold, G Battaglin, R Bertoncello and F Gonella, *Nucl. Instrum. Methods* **B91**, 478 (1994) and references therein
[6] A Carnera, P Mazzoldi, A Boscolo-Boscoletto, F Caccavale, R Bertoncello, G Granozzi, I Spagnol and G Battaglin, *J. Non-Cryst. Solids* **125**, 293 (1990)
[7] G W Arnold, R K Brow and D R Myers, *J. Non-Cryst. Solids* **120**, 234 (1990)
[8] H Hosono, Y Abe, K Oyoshi and S Tanaka, *Phys. Rev.* **B43**, 1193 (1991)
[9] P Mazzoldi, A Carnera, F Caccavale, M L Favaro, A Boscolo-Boscoletto, G Granozzi, R Bertoncello and G Battaglin, *J. Appl. Phys.* **70**, 3528 (1991)
[10] R Bertoncello, A Glisenti, G Granozzi, G Battaglin, F Caccavale, E Cattaruzza and P Mazzoldi, *J. Non-Cryst. Solids* **162**, 205 (1993)
[11] R Bertoncello, F Trivillin, E Cattaruzza, P Mazzoldi, G W Arnold and G Battaglin, *J. Appl. Phys.* **77**, 1294 (1995)
[12] E Cattaruzza, G Mattei, P Mazzoldi, R Bertoncello, G Battaglin, and L Mirenghi, *Appl. Phys. Lett.* **67**, 2884 (1995)
[13] E Cattaruzza, R Bertoncello, F Trivillin, P Mazzoldi, G Battaglin, L Mirenghi and P Rotolo, *J. Mater. Res.* **11**, 229 (1996)
[14] P Mazzoldi, G W Arnold, G Battaglin, F Gonella and R F Haglund Jr., *J. Nonlinear Opt. Phys. Mater.* **5**, 285 (1996)
[15] P Mazzoldi, F Caccavale, F Gonella and G Battaglin, *J. Opt. Technol.* **62**, 817 (1995)
[16] O Knacke, O Kubaschewski and K Hesselman (eds), *Thermochemical Properties of Inorganic Substances*, 2nd ed. (Springer-Verlag, Berlin, Heidelberg, 1991)
[17] G W Arnold, G Battaglin, A Boscolo-Boscoletto, F Caccavale, G De Marchi, P Mazzoldi and A Miotello, *Nucl. Instrum. Methods* **B65**, 387 (1992)
[18] R Pretorius, J M Harris and M-A Nicolet, *Solid-State Electron.* **21**, 667 (1992)
[19] R Kelly, *Mater. Sci. Eng.* **A115**, 11 (1989)
[20] G W Arnold and J A Borders, *J. Appl. Phys.* **48**, 1488 (1977)
[21] G Battaglin, G Della Mea, G De Marchi, P Mazzoldi and A Miotello, *Nucl. Instrum. Methods* **B1**, 511 (1984)
[22] F Geotti-Bianchini, P Polato, S Lo Russo and P Mazzoldi, *J. Am. Ceram. Soc.* **67-1**, 39 (1984)
[23] G Ottaviani, *Thin Solid Films* **140**, 3 (1986)